Layering and orientational ordering of propane on graphite: An experimental and simulation study

Xiongce Zhao
Department of Chemical and Petroleum Engineering, University of Pittsburgh, Pittsburgh, Pennsylvania 15261

Seokjoon Kwon
Department of Civil and Environmental Engineering and Surface Science Center, University of Pittsburgh, Pittsburgh, Pennsylvania 15260

Radisav D. Vidic
Department of Civil and Environmental Engineering, University of Pittsburgh, Pittsburgh, Pennsylvania 15261

Eric Borguet
Surface Science Center, and Department of Chemistry, University of Pittsburgh, Pittsburgh, Pennsylvania 15261

J. Karl Johnson[a)]
Department of Chemical and Petroleum Engineering, University of Pittsburgh, Pittsburgh, Pennsylvania 15261 and National Energy Technology Laboratory, Pittsburgh, Pennsylvania 15236

(Received 1 May 2002; accepted 30 July 2002)

We report the results of an experimental and theoretical study of propane adsorption on highly oriented pyrolytic graphite. Simulations and experiments were carried out for temperatures from 90 to 110 K and pressures from ultrahigh vacuum up to about 0.5 mTorr. Both simulations and experiments show that propane adsorbs in a layer-by-layer fashion and exhibits continuous growth beyond the second layer at the higher temperatures studied. Experimental adsorption data were obtained by optical differential reflectance (ODR) and temperature programmed desorption (TPD). The ODR method is able to dynamically follow the adsorption and desorption process as a function of time over a wide pressures range, while TPD probes only the desorption events at ultrahigh vacuum conditions. The influence of the fluid–fluid potential on the adsorption isotherms has been investigated by comparing simulations using five different propane potentials. The pressure at which the second layer forms was found to vary by more than 1 order of magnitude among the potentials tested, whereas the isosteric heat of adsorption is less sensitive to the potential. We find that the propane potential that best describes the liquid phase energetics is in the best agreement with experimental adsorption isotherms and isosteric heats. The binding energy of propane in the monolayer measured from TPD experiments is in excellent agreement with that computed from simulations, both giving values of about 30 $kJ\,mol^{-1}$. The isosteric heat of adsorption at incipient second layer formation is $23\pm2\ kJ\,mol^{-1}$ as measured from ODR isotherms and $24\pm1\ kJ\,mol^{-1}$ computed from simulations. The isosteric heat as a function of coverage computed from molecular simulations is roughly constant over the 1–2 and the 2–3 layering transitions at 91 K. We show that this unusual behavior is due to a rotational transition, whereby molecules in the first layer rotate from a parallel (all CH_x groups in contact with the graphite plane) to a perpendicular (one CH_3 group pointing up) orientation. This rotational transition has two effects: it allows more molecules to adsorb in the monolayer and increases the isosteric heat of adsorption in the second layer over that for adsorption onto an atomically smooth surface. © *2002 American Institute of Physics.*
[DOI: 10.1063/1.1508363]

I. INTRODUCTION

The adsorption of airborne pollutants (e.g., acids, organics, and metal vapors) on carbonaceous surfaces, such as activated carbon, has attracted much experimental and theoretical interest in the past few decades.[1,2] The adsorption of organic molecules on carbonaceous surfaces is also of importance in many industrial processes ranging from water and air purification[3] to lubrication and protection of surfaces of magnetic data storage media.[4] However, there is still a lack of fundamental understanding of the surface physics and chemistry of carbonaceous surfaces and how these affect simple processes such as adsorption and desorption.

Many experimental studies have been performed on the adsorption of hydrocarbons on activated carbons.[5] However, given the lack of knowledge of the structure of activated

[a)]Author to whom correspondence should be addressed. Electronic mail: karlj@pitt.edu

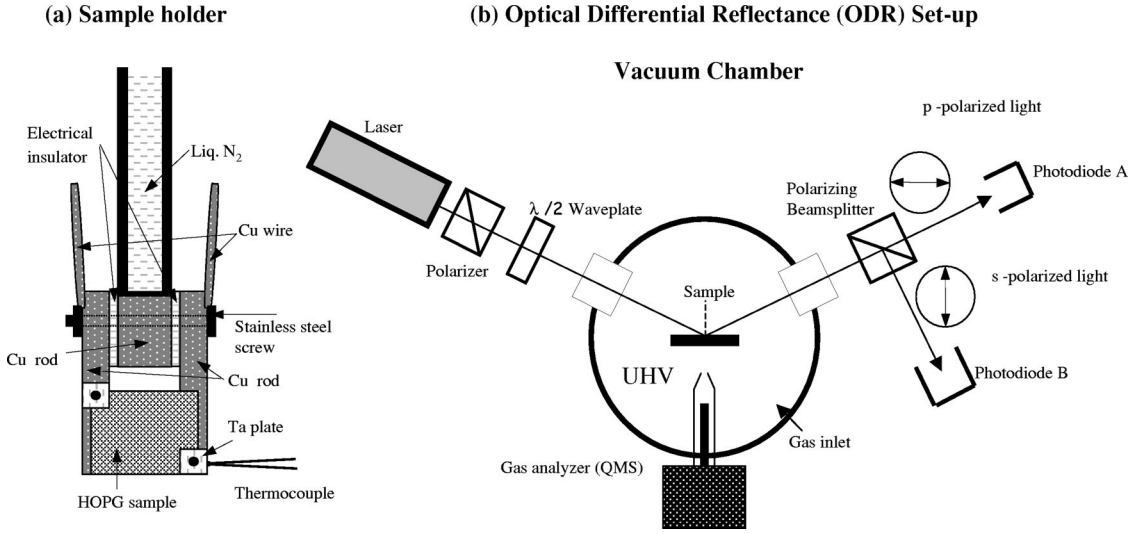

FIG. 1. Experimental setup for ODR and TPD: (a) sample holder and (b) vacuum chamber and instrumentation.

carbon it is difficult to draw conclusions about the fundamental surface interactions or the relative importance of pore size distribution, pore connectivity, and sorbate heterogeneity as they relate to the the adsorption process. There are relatively few fundamental studies on the adsorption of alkanes on well characterized surfaces, such as highly ordered pyrolytic graphite (HOPG). However, the adsorption of simple fluids (e.g., methane, noble gases) on graphitic surfaces has been studied extensively.[6–10] Studies of adsorption of polar and other more complex molecules on graphite have mainly focused on the monolayer structure rather than layering transitions,[11,12] although some multilayer studies have been performed.[13,14] Recent work by Paserba and Gellman explored fundamental interactions between *n*-alkanes and HOPG.[15,16] The monolayer structures of hydrocarbons adsorbed on HOPG have been investigated by scanning tunneling microscopy.[17] Layering transitions and layer critical points have been observed for methane, ethane, and ethylene on graphite[10,18–21] but there have been no studies of layering transitions of propane on graphite. The melting of monolayer propane on graphite has been measured experimentally and found to be very weak and broad, with the peak in the heat capacity occurring at about 67 K.[22] Matthies measured the structure of the propane monolayer on graphite using both neutron and x-ray diffraction but was unable to fit the experimental data to any reasonable structure.[23]

Molecular simulation studies on the adsorption of alkanes on solid surfaces focused primarily on modeling porous sorbents, such as graphite slit pores, ideal cylindrical pores,[24–29] porous glass,[30,31] microporous carbons,[32,33] and zeolitic materials.[34–50] There have been extensive simulations of adsorbed fluids and solids on graphite surfaces, with most simulations performed for relatively simple molecules.[7,24,25,51,52] A few simulations of the adsorption quantum fluids (hydrogen, helium) on graphite have been carried out.[53–57] Relatively few simulations of adsorption of higher alkanes on graphitic and other surfaces have been performed.[58–62] Most of these simulations have addressed structural and melting transitions in the monolayer; none of these studies have investigated layering transitions.

Propane is one of the most important lower hydrocarbons and has received significant research attention. Several experimental studies have been performed to determine general features of high pressure physical adsorption on homogeneous high energy solid surfaces at ambient temperature.[63–65] In theoretical studies, Cracknell and Nicholson[26–28] calculated isosteric heat of adsorption at zero coverage of propane and ethane on graphite at ambient temperatures. Their results were in excellent agreement with experimental data. However, no experimental or theoretical work has been done on the adsorption behavior of propane on graphite at low temperatures and vacuum pressures. An understanding of such a simple model system is a prerequisite to the investigation of more complex carbonaceous systems important in atmospheric processes, catalysis, adsorption, and lubrication.

In this paper we present experimental measurements and calculations of propane adsorption on HOPG. The temperature range evaluated in this study is from 90 to 110 K (the freezing point of bulk propane is 84.5 K[66]), while the pressure spans a range of 6 orders of magnitude from 5×10^{-10} to 5×10^{-4} Torr. Theoretical isotherms and isosteric heats of adsorption are compared with experimental data. We show that potential models which accurately describe the condensed phase fluid–fluid energetics are required to give good agreement of adsorption isotherms and isosteric heats with experimental values. An orientational ordering transition is observed from simulations for propane in the monolayer.

II. EXPERIMENT

A stainless steel ultrahigh vacuum (UHV) chamber equipped with a turbomolecular pump backed by a mechanical pump provides a base pressure of 5×10^{-10} Torr after bakeout. A copper block mounted on a stainless steel liquid nitrogen reservoir holds two electrically isolated copper rods as sample supports [Fig. 1(a)]. The temperature of the sample can be controlled between 87 and 1273 K and is

measured with a *K*-type thermocouple welded to the sample fixing plate and wedged against the HOPG sample. The location of the thermocouple is a compromise as it cannot be spot welded directly to the sample. We estimate that the precision of the temperature readings is ± 1 K. The pressure in the chamber is measured by an ion gauge and is reported as uncorrected ion gauge readings.

The substrate was (10 mm$\times$10 mm$\times$0.25 mm) HOPG, grade SPI-1 supplied by SPI. Additional experiments were performed on a different sample supplied by Advanced Ceramics (HOPG, grade ZYA). Atomic force microscopy images of both the SPI and Advanced Ceramics samples look very similar and temperature programmed desorption (TPD) results on the two samples were similar. The sample was cleaved using adhesive tape prior to installation in the UHV chamber. After bakeout, the sample was annealed to 1273 K to remove possible contamination.[67] Gas exposure was performed by backfilling the chamber and reported in Langmuir ($1\ \mathrm{L}=10^{-6}$ Torr s) as determined from uncorrected ion gauge readings. TPD experiments were performed using a quadrupole mass spectrometer (QMS) (Stanford Research, AccuQuad300). The QMS shield aperture could be repeatedly positioned to within 1 mm of the sample and retracted about 20 mm to allow sample rotation and dosing. Temperature, pressure, and optical reflectivity change were monitored via a PC with analog to digital converter board. The QMS signal (at $m/e=44$ amu) integrated over the desorption temperature range gives the relative amount of propane adsorbed.

The optical setup for measuring the reflectivity change induced by surface adsorption and desorption is illustrated in Fig. 1(b). The chamber is equipped with several viewports for laser light access to the sample. The light source is a laser pointer (Marlin P. Johnson Assoc. Inc., Model No. 8689-LZ). After passing through a polarizer (Lambda Research Optics Inc., Model No. ppb-2506u-248), a half wave plate (Lambda Research Optics Inc., Model No. WP-10QC-M) on a rotatable mount, the laser beam strikes on the sample at a 65° ($\pm 1°$) angle of incidence. The light beam reflected from the sample is divided into *p*- and *s*-polarized light components with a polarizing beam splitter (Coherent, Model No. 44-4703). Each component is detected separately by its own photodiodes (THORLABS Inc., Model No. DET 110). The *p*-polarized light is the signal and the *s*-polarized light is used as the reference due to the fact that adsorbate-induced reflectivity change depends on polarization with *p*-polarized light being far more sensitive than *s*-polarized light to the presence of the adsorbate.[13]

Prior to experiments reported here, the sample used in optical differential reflectance (ODR) experiments was initially cleaned by heating up to 1000 K and cooled back to the desired temperature for adsorption (90–110 K). The intensities of reflected *p*- and *s*-polarized light were initially equalized by adjusting the half wave plate. The sample is exposed to propane gas by backfilling the chamber to a desired pressure. Typically, the pressure is increased from $<10^{-9}$ to $>10^{-4}$ Torr over about 1 min. The reversibility of each observed change in ODR is determined by reducing the pressure to see if the ODR signal reverses. After completing the adsorption step, the temperature of the sample is ramped for desorption, typically at 2.5 K/s.

TABLE I. Parameters for the propane potential models used in this work.

	LS	OPLS	SKS	TraPPE	NERD
δ_{CC}(Å)[a]	2.16	1.53	1.54	1.54	1.54
θ_{CCC}[b]	90°	112°	114°	114°	114°
σ_{CH_2}(Å)	3.527	3.905	3.93	3.95	3.93
σ_{CH_3}(Å)	3.527	3.905	3.93	3.75	3.857
ϵ_{CH_2}/k_B(K)	119.57	59.4	47	46	45.8
ϵ_{CH_3}/k_B(K)	119.57	88.1	114	98	102.6

[a] δ_{CC} is the bond length between CH_2 and CH_3.
[b] θ_{CCC} is the bond angle.

III. MOLECULAR SIMULATION

There are two kinds of interactions involved in simulation of adsorption, namely, fluid–fluid and solid–fluid interactions. The contribution of fluid–fluid interactions to the total energy of adsorption increases with coverage. Thus, the fluid–fluid potential will not affect the shape of the adsorption isotherm at very low coverage (Henry's law region), but will have profound effect at higher loadings. In this study we have investigated five different propane potential models, namely, the Lustig and Steele[68] (LS), OPLS,[69] TraPPE,[70] NERD,[71] and SKS[72] models. All of these potentials are based on a united-atom description of propane but they differ in the geometry of the propane molecule and the potential parameters.

In all five potential models the interaction between two sites *i* and *j* on two different propane molecules are described by pairwise-additive Lennard-Jones potentials

$$u(r_{ij})=4\epsilon_{ij}\left[\left(\frac{\sigma_{ij}}{r_{ij}}\right)^{12}-\left(\frac{\sigma_{ij}}{r_{ij}}\right)^{6}\right], \tag{1}$$

where r_{ij}, ϵ_{ij}, and σ_{ij} are the site–site separation, energy parameter, and size parameter, respectively, for the two sites. The interaction parameters for different models are listed in Table I. Parameters for the cross interactions are obtained using the Lorentz–Berthelot combining rules

$$\sigma_{ij}=\frac{\sigma_i+\sigma_j}{2}, \tag{2}$$

$$\epsilon_{ij}=(\epsilon_i\epsilon_j)^{1/2}. \tag{3}$$

We have calculated the thermodynamic properties of pure propane at several different liquid and vapor state points using the five different potentials in order to test their accuracy. The simulation pressures were computed from ensemble averages of the pressure virial.[73] The calculated and experimental pressures are shown in Table II. All simulations were carried out in the canonical (*NVT*) ensemble at the experimental temperatures and densities. The bulk system consisted of 610 molecules and was equilibrated for 1.5×10^6 steps and data were collected over 5×10^5 steps. All the potentials were truncated at $5\sigma_{ff}$ and no long-range corrections were applied. The authors of SKS and TraPPE models suggested that an accurate calculation of thermodynamic properties of propane using these potentials requires a cutoff of

TABLE II. Comparison of liquid and gas phase pressures for propane from experiment and calculated from the five potentials listed in Table I. The simulations were performed in the *NVT* ensemble.[a]

			Simulated pressure (MPa)				
T(K)	ρ (kg m^{-3})	P_{ex} (MPa)	LS	OPLS	TraPPE	SKS	NERD
Gas							
200	0.2667	0.01	0.010 012(1)	0.010 035(8)	0.010 014(6)	0.009 994(7)	0.010 009(1)
300	0.1771	0.01	0.010 003(3)	0.010 039(2)	0.010 007(2)	0.009 997(3)	0.010 004(3)
300	1.7955	0.1	0.099 90(1)	0.100 48(6)	0.100 21(1)	0.099 47(1)	0.099 97(7)
AAD[b]			8.3×10^{-6}	4.1×10^{-5}	1.4×10^{-5}	2.0×10^{-5}	5.3×10^{-6}
Liquid							
100	718.94	0.01	12(3)	144(2)	13(2)	252(7)	113(2)
200	615.98	0.1	7(3)	56(2)	7(2)	57(2)	34(2)
250	559.46	1.0	1.2(3)	31(2)	7(2)	23(2)	34(2)
300	492.49	2.0	−0.2(1)	18(1)	7(1)	4(2)	9(1)
AAD[b]			5.3	61.5	7.7	83.3	46.7

[a]The numbers in parentheses represent uncertainties in the last digit.
[b]Average absolute deviation, defined as AAD$=(1/N)\,\Sigma_{i=1}^{N}|P_i^{\exp}-P_i^{\mathrm{sim}}|$.

more than 30 Å for temperatures as low as about 100 K.[74] Using such a long cutoff would make the simulation of the liquid very expensive. However, we ran simulations with a cutoff of $3.5\sigma_{ff}$ (about 14 Å) and $5\sigma_{ff}$ (about 20 Å) to calculate the internal energy of liquid propane in the temperature range of 90–180 K, and found that the differences in the internal energies from these two cutoffs are typically about 1%.

The simulated pressures are compared with experimental data.[75] As shown in Table II, all five models predict accurately the gas phase pressures while none reproduces the liquid pressures. This is not surprising because the incompressibility of liquids means that a small error in the potential may lead to a very large error in the computed liquid pressures.

We have also calculated the internal energy U of liquid propane at 0.01 MPa as a function of temperature using these potentials. The values obtained were compared with the results from the modified Benedict–Webb–Rubin (MBWR) equation of state (EOS),[66] the parameters of which were regressed from experimental data. The results are plotted in Fig. 2. We found that the LS model gives the best agreement with the MBWR EOS data.

We note that only the LS model was specifically designed for propane while the other four potentials were developed from a universal description of *n*-alkanes. The LS model was designed to reproduce the PVT properties of propane, not the energetic properties, so it is somewhat surprising that it is superior to the other models for predicting internal energy, especially given the unrealistic bond lengths and bond angle used in the LS model. Nevertheless, because of its success, as illustrated in Fig. 2, we adopted the LS potential as the basic model throughout our adsorption simulations. The other four potentials were used to compute a single isotherm in order to assess the effect of the fluid–fluid potential on the isotherm.

The graphite surface is modeled as a smooth basal plane. The interaction energy between a propane molecule and graphite surface is given by the 10-4-3 potential[76]

$$u_{sf}(z)=2\pi\epsilon_{sf}\sigma_{sf}^2\Delta\rho_s\left[\frac{2}{5}\left(\frac{\sigma_{sf}}{z}\right)^{10}-\left(\frac{\sigma_{sf}}{z}\right)^{4}-\frac{\sigma_{sf}^4}{3\Delta(0.61\Delta+z)^3}\right], \tag{4}$$

where z is the distance between a fluid molecule interaction site and the graphite surface, ρ_s is the graphite number density, and Δ is the distance between the graphene sheets in graphite. The solid–fluid interaction parameters ϵ_{sf} and σ_{sf} are calculated from the Lorentz–Berthelot rules. The values of the parameters are: $\rho_s=114$ nm^{-3}, $\Delta=0.335$ nm, $\epsilon_s/k_B=28.0$ K, and $\sigma_s=0.340$ nm.[26]

We have used grand canonical Monte Carlo (GCMC) simulations to compute the isotherms and isosteric heats. A detailed description of the GCMC technique can be found elsewhere.[73] In GCMC, the temperature T, the volume of the

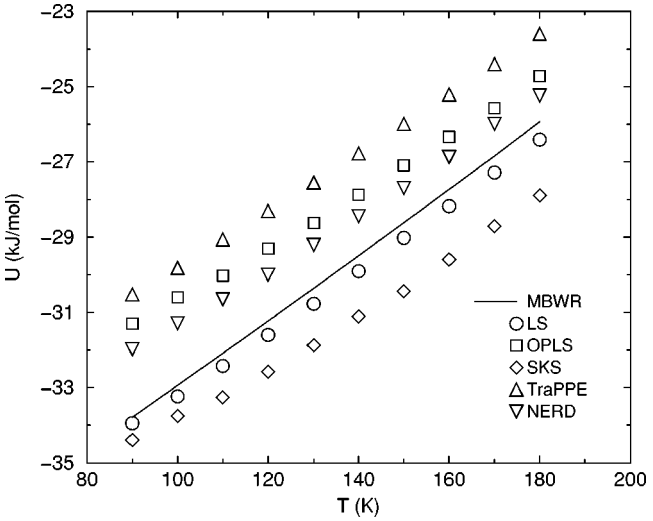

FIG. 2. Internal energy of liquid propane calculated from the MBWR equation of state (Ref. 65) (line) and simulations at 0.01 MPa. The symbols are from simulations using the five potentials listed in Table I.

simulation cell V, and the chemical potential μ, are held constant. The number of molecules in the cell is allowed to vary and the average value represents the absolute amount of gas adsorbed.

Four kinds of moves are involved in GCMC simulation of propane on graphite: (i) displacement of the center of mass of a molecule, (ii) rotation of a molecule, (iii) creation of a molecule, and (iv) deletion of a molecule. Periodic boundary conditions and minimum image conventions were applied in the x and y directions of the simulation box. The dimensions of the simulation box were equal in the x and y directions and ranged from 10 to $15\sigma_{\mathrm{ff}}$, which gave average numbers of adsorbed molecules ranging from 70 to 350. The bottom wall of the simulation box was chosen as the adsorbing surface and the opposite wall was chosen to be purely repulsive to keep the molecules in the box. The separation between the two walls was fixed at $20\sigma_{\mathrm{ff}}$ so that the influence of the repulsive wall on the adsorption properties was negligible. The site–site interaction cutoff distance was $5\sigma_{\mathrm{ff}}$ and no long-range corrections were applied. The probabilities of making a displacement, rotation, deletion, and creation were each set to 0.25. The maximum values of displacement and rotation were adjusted during the equilibration to achieve acceptance ratios for displacements and rotations of about 0.4.

Simulations were performed at temperatures of 91, 95, 100, 105, 110, and 300 K. The low temperature simulations ($T \leqslant 110$ K) were equilibrated for 5×10^7 moves, after which data were collected for another 5×10^7 moves. Simulation statistics at 300 K were much better so that only 2×10^6 moves for equilibration and data collection were required.

The isosteric heat of adsorption can be computed directly in a GCMC simulation from the fluctuations of the number of molecules and the energy[77]

$$q_{\mathrm{st}} = kT - \frac{\langle UN\rangle - \langle U\rangle\langle N\rangle}{\langle N^2\rangle - \langle N\rangle^2}, \tag{5}$$

where q_{st} is the isosteric heat of adsorption per molecule, U is the total potential energy of the system, and N is the number of molecules in the simulation cell.

Experimental adsorption isotherms are usually measured in terms of the excess amount adsorbed as a function of the pressure of the bulk fluid in equilibrium with the adsorbed fluid, while the simulations give absolute amounts adsorbed. The excess adsorption is given by

$$n^e = n - V^a\rho^g, \tag{6}$$

where n^e and n are the excess and total (absolute) adsorption, respectively, V^a is the volume in the system that can be occupied by gas molecules, and ρ^g is the density of the bulk gas at the system temperature and pressure. Note that V^a excludes the volume of the solid sorbent. The absolute and excess adsorption are virtually identical at the low pressures considered in this study. We obtained the bulk pressures for each chemical potential by assuming ideal gas behavior in the bulk. This is an excellent approximation given the range of pressures covered. We have also performed GCMC simulations of bulk propane at several state points to verify the accuracy of the ideal gas law approximation. The results from these two approaches were found to agree within the simulation errors.

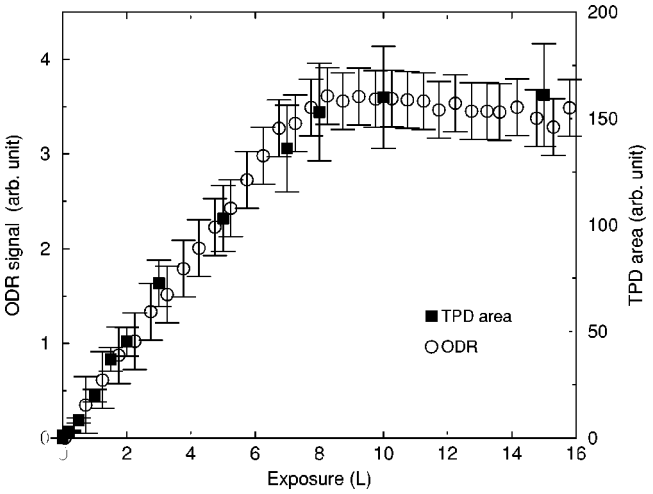

FIG. 3. Integrated TPD area (squares) and ODR signal (circles) as a function of exposure, measured in Langmuir ($1\ \mathrm{L} = 10^{-6}$ Torr s).

IV. RESULTS AND DISCUSSION

A. Adsorption isotherms

We have performed both TPD and ODR experiments for propane adsorption on HOPG. The TPD method has been used extensively for studying both chemisorption and physisorption and is considered to be very accurate for determining relative coverage. The ODR method is not as widely used, especially for physisorption systems. In order to validate ODR as a quantitative technique the optical reflectivity change should correlate with coverage as determined from TPD. Figure 3, a plot of the ODR signal and TPD area as a function of a common exposure, shows excellent agreement between these techniques. Both the ODR signal and TPD area saturate at around 8 L. The excellent correlation of the ODR signal and the TPD area indicates that ODR accurately measures the surface coverage change induced by monolayer adsorption. The agreement also indicates that the TPD spectra are free from contributions due to desorption from other surfaces in the chamber because ODR only probes a small area ($<1\ \mathrm{mm}^2$) in the center of the HOPG sample.

The ODR measurements were performed to determine the reversibility of bilayer formation. The ODR signal change as a function of propane pressure at 90 K is provided in Fig. 4. The different symbols on the figure describe the sequence of propane pressure adjustment and its adjustment direction (increase or decrease). The propane pressure was initially increased from UHV to about 5×10^{-6} Torr (squares) and then reduced to below 10^{-7} Torr (triangles). Finally, the propane pressure was increased to above 1×10^{-5} Torr while the ODR signal was recorded. The initial signal growth in the lower pressure region (up to 2×10^{-7} Torr) in Fig. 4 suggests monolayer adsorption, as verified by TPD and simulations. The signal in the submonolayer regime does not represent an equilibrium condition. The coverage increases with increasing time as the pressure

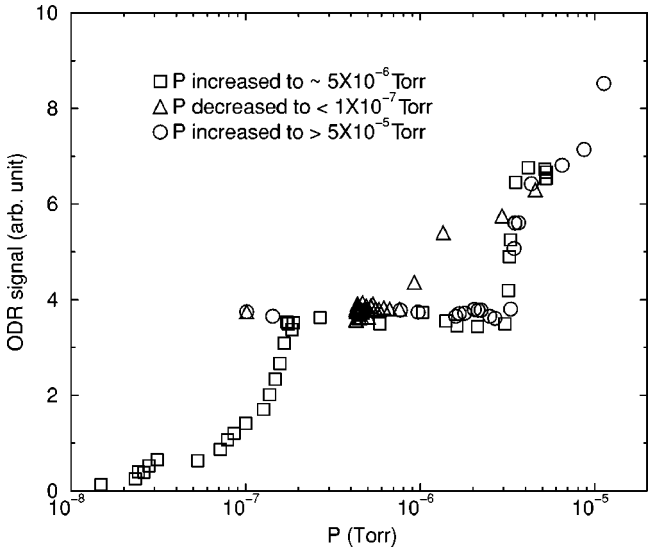

FIG. 4. ODR signal change induced by propane pressure at 90 K. The legend indicates the direction of the propane pressure adjustment. Squares correspond to an initial pressure of $<10^{-9}$ Torr and increasing pressure to 5×10^{-6} Torr. Triangles correspond the subsequent pressure decrease from 5×10^{-6} to $<10^{-7}$ Torr, and the circles correspond to an increase from to $<10^{-7}$ to $>10^{-5}$ Torr.

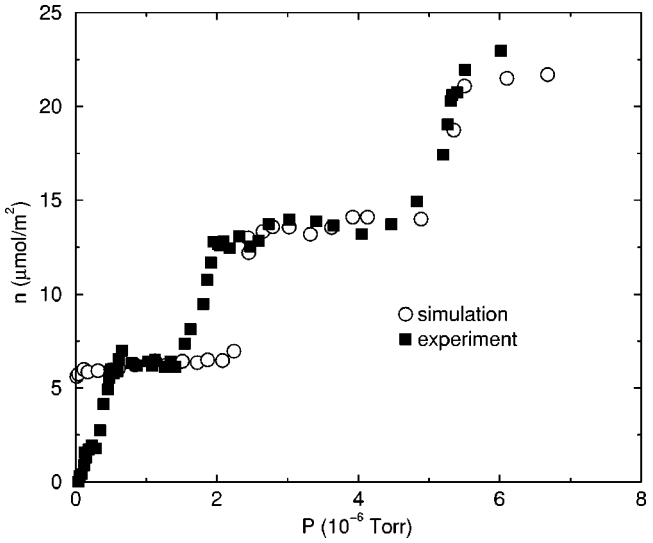

FIG. 5. Adsorption isotherms from experiment and simulation at 91 K. The filled squares are experimental data, the open circles are GCMC results. The simulations report the absolute adsorption, which at these pressures is virtually identical to the excess adsorption. The experimental data are measured in arbitrary units and scaled to match the first layer coverage from simulations.

is increased from UHV to about 10^{-7} Torr. Hence, the initial rise in coverage shown in Fig. 4 reflects the kinetics of the dosing process. We assume that the signal increase for propane pressures between 3×10^{-6} and 5×10^{-6} Torr is induced by bilayer formation. This assumption is supported by the simulations. The reversibility of bilayer formation can be clearly seen from the ODR signal decrease to the monolayer ODR signal level when the pressure is reduced to under 1×10^{-7} Torr. However, the ODR signal remained at the level induced by the monolayer formation, although the propane pressure was reduced below the pressure at which monolayer formation occurred. Such behavior suggests that the propane monolayer adsorption is not reversible on the time scale of our measurements at 90 K. Bilayer formation is only observed above a critical pressure of about 3×10^{-6} Torr. Surface coverage increases when the rate of molecular adsorption is greater than the rate of desorption. This occurs at pressures over 3×10^{-6} Torr, when the total flux of propane molecules is 6.31×10^{14} cm^{-2} s^{-1} as calculated by the kinetic theory.[78] Multilayer condensation is observed at over 1×10^{-5} Torr of propane total pressure (circles). Multilayer formation is also reversible, as the ODR signal returned to the monolayer coverage when the pressure was brought back below 1×10^{-6} Torr (not shown here).

Propane isotherms at about 90, 95, 100, 105, and 110 K were obtained in our experimental study. A distinct bilayer transition (apparently first order) was observed for the experiments at 105 K and below. No layering transition was observed in the 110 K experiment because the pressure was not high enough. The pressures at which the bilayer begins to form were found to be 2.4×10^{-6}, 2.3×10^{-5}, 6.2×10^{-5}, and 2.4×10^{-4} Torr, for 90, 95, 100, and 105 K, respectively. These transition pressures are average values from several runs. The estimated uncertainty in the absolute pressure at which the bilayer forms is about 30%, while the uncertainty in the relative temperature is about ±1 K. These uncertainties were determined by calculating the standard deviation from several experiments. Two representative experimental isotherms, along with data from GCMC simulations, are shown in Figs. 5 and 6. The observation of the formation of the bilayer and multilayer was enabled by the use of ODR. Although TPD is a widely used surface analysis technique, it is not suitable to observe the states that are reversibly populated, i.e., states that require high ambient pressure to be observed. The reduction in pressure required to perform TPD depopulates bilayer and multilayer states, hence the absence of the corresponding peaks in TPD spectra on Fig. 7.

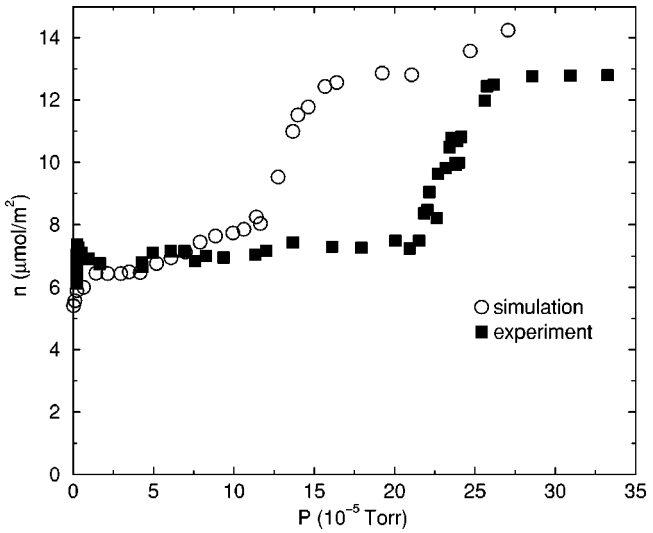

FIG. 6. Adsorption isotherms from experiment and simulation at 105 K. The filled squares are experimental data, the open circles are GCMC results.

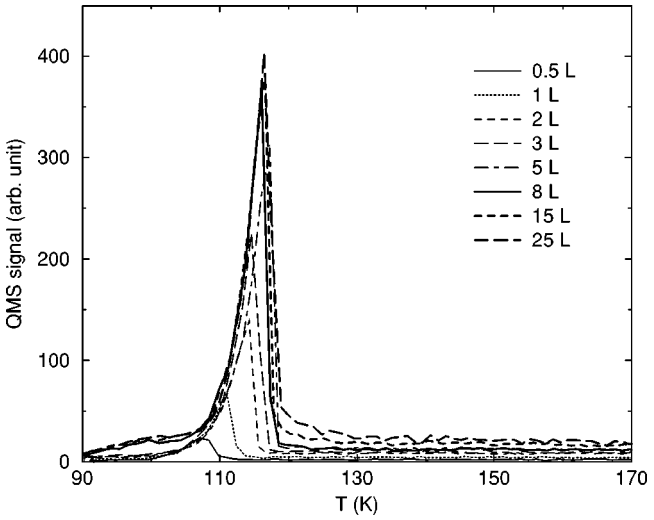

FIG. 7. TPD spectra of propane from HOPG following propane exposures ranging from 0.5 to 25 L at 90 K. A single peak grows at around 115 K and saturates above 8 L exposure.

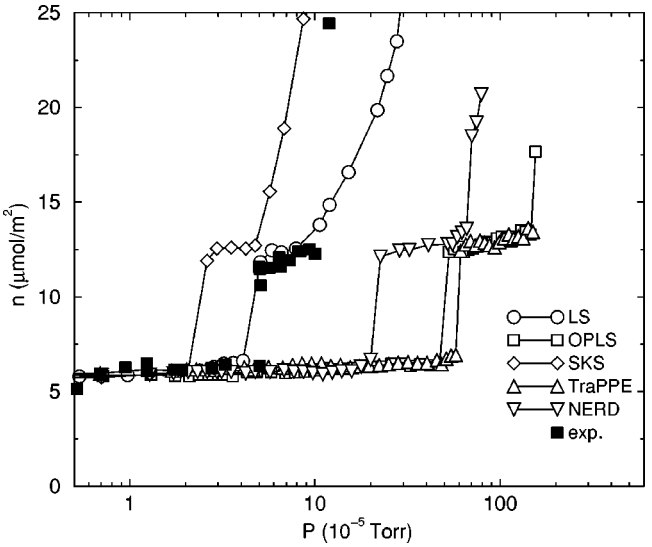

FIG. 8. Adsorption isotherms at 100 K from five different propane potential models and experiments. The filled squares are from experiments. The open circles, squares, diamonds, up triangles, and down triangles are from the LS, OPLS, SKS, TraPPE, and NERD potentials, respectively. The lines are drawn to guide the eye.

In Fig. 5, we present the adsorption isotherm data for propane on HOPG at 91 K determined from experiments and simulations. The experimental adsorption loadings were measured in arbitrary units and converted to μmol/m^2 by matching the monolayer loading with the simulation data. Because the relative adsorbed amounts measured experimentally are accurate, the good agreement between experiments and simulations for the second layer loadings indicate that simulations accurately predict relative coverages in the first and second layers. The position of the first to second layer transition on the pressure axis determined from experiments and simulations are in very good agreement. The agreement, however, is probably fortuitous because of the experimental difficulty in measuring the absolute pressure accurately. Furthermore, transition pressures are very sensitive to substrate temperature. While relative temperature precision is about 1 K, absolute temperature is measured less accurately. We are unable to observe a transition from zero loading to the first layer in any of the simulations. We obtained virtually complete monolayer coverage at the lowest pressures simulated (about 2×10^{-8} Torr), indicating that the 0–1 transition must occur at pressures lower than 2×10^{-8} Torr. The apparent 0–1 layering transition seen in the experimental data (e.g., Figs. 5 and 6) is the result of kinetic effects, as discussed above. The pressure in the UHV chamber was rapidly increased before the monolayer had a chance to form completely and the experimental data below the monolayer coverage in Fig. 5 do not reflect true equilibrium. The kinetic nature of the ODR data can also be inferred from the data in Fig. 4, which shows that the first layer remains intact upon reduction of the pressure. Indeed, we find that if the first layer cannot be removed over a reasonable time by evacuating the chamber; the substrate must be heated to remove the first layer (see Fig. 7). These data reflect the dynamic nature of adsorption experiments, i.e., it takes a finite time to form a monolayer at a fixed pressure. These data do not reflect metastable states. The simulations, however, reflect equilibrium (or metastable) conditions.

Experimental and simulation isotherms for 105 K are shown in Fig. 6. The 1–2 layering transition pressures from simulation and experiment do not agree as well as in the 91 K case, but they are in good qualitative accordance. The relative coverages in the first and second layer are in excellent agreement.

We have investigated the effect of the fluid–fluid potential model on the adsorption isotherm by computing the 100 K isotherm for all five propane potential models examined in this study. The results of these calculations are plotted together with experimental data in Fig. 8. The most striking observation in Fig. 8 is that the transition pressure for the 1–2 layering transition computed using the different fluid–fluid potentials varies by more than 1 order of magnitude, which is significantly more than the difference observed between our experimental data and simulation data obtained using the LS potential. The SKS potential exhibits the lowest transition pressure of about 2×10^{-5} Torr, while the TraPPE potential gives the highest transition pressure of about 6×10^{-4} Torr.

Comparing Figs. 2 and 8, we see that the sequence of the 1–2 layering transition pressures at 100 K for different propane models exactly follows the ordering of internal energy values for liquid propane. For example, the liquid propane internal energy calculated by the SKS model is the lowest in Fig. 2 and consequently, the transition pressure predicted by the SKS model in Fig. 8 is the smallest. The coincidence of liquid internal energies with the order of the transition pressures is due to the important role of the fluid–fluid interactions in simulating the 1–2 layering transition. It is noted that about a 10% difference in U (comparing SKS with TraPPE in Fig. 2) gives rise to more than a 1 order of magnitude change in the transition pressure, while having apparently no effect on the sharpness of the transition. We have computed the isosteric heats of adsorption for the 100 K isotherm using each of the five fluid–fluid potentials listed in Table I. The

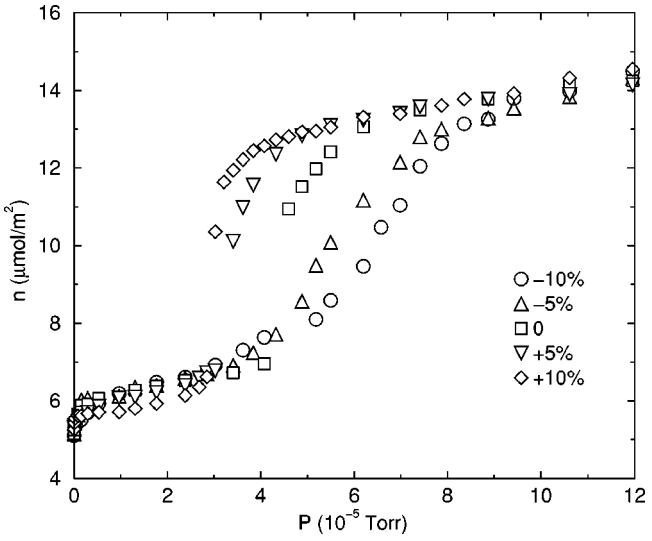

FIG. 9. Adsorption isotherms at 100 K using the LS fluid–fluid potential and different values of ϵ_{sf}. The squares denote the standard ϵ_{sf}, the circles (diamonds) denote an increase (decrease) of 10% in ϵ_{sf}, and the up (down) triangles denote an increase (decrease) of 5%. All the simulations in this figure were performed with a cutoff of 3.5σ.

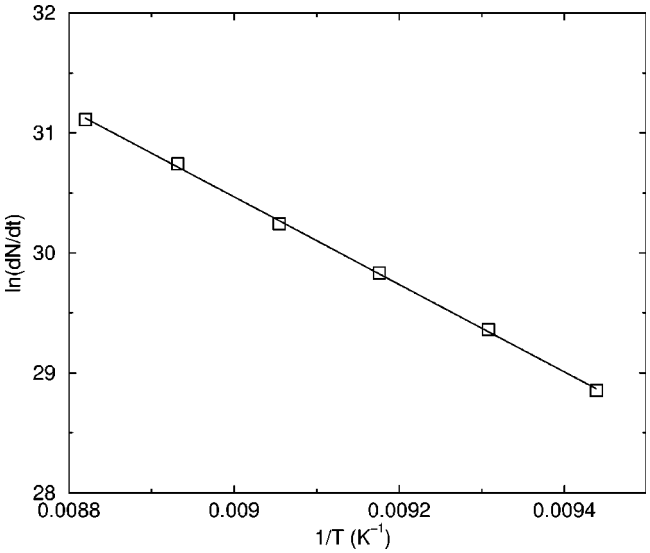

FIG. 10. Calculation of activation energy for propane on HOPG using zero order desorption kinetics. The propane exposure is 25 L. The squares represent experimental data and the solid line is a fit to the data. The average activation energy determined from multiple experiments is 30 ± 2 kJ mol^{-1}.

values of q_{st} were computed from Eq. (5). We note that the differences in the fluid–fluid potentials have a relatively small effect on the values of q_{st} when compared with the transition pressures. The large statistical uncertainties in the simulation data tend to mask the differences due to the potentials.

We note that changing the fluid–fluid potential implicitly changes the solid–fluid potential through changes in the geometry of the molecule and through the combining rules of Eqs. (2) and (3). We have studied the effect of changing only the solid–fluid potential by computing the 100 K isotherm using the LS fluid–fluid potential, while changing ϵ_{sf} in Eq. (4) by $\pm5\%$ and $\pm10\%$. The results of these calculations are plotted in Fig. 9. Note that perturbing the solid–fluid potential has a much smaller effect on the location of the 1–2 layering transition pressure than the effect of changing the fluid–fluid potential (compare Figs. 8 and 9). An increase (decrease) of 10% in the solid–fluid potential leads to roughly a factor of 2 decrease (increase) in the transition pressure. We note that the shape of the isotherm is a fairly strong function of the solid–fluid potential. A decrease in ϵ_{sf} of only 5% appears to change the 1–2 layering transition from first order to continuous, as can be seen from the shape of the isotherm. This is surprising because one would expect the 1–2 layering transition to be less sensitive to small perturbations in the solid–fluid potential given that the magnitude of the potential is attenuated roughly by a factor of 0.1 in the second layer compared with the first layer due to the increased distance from the graphite plane.

B. Adsorption energetics

As noted above, the desorption of the second layer of propane is reversible, i.e., it can be achieved by lowering the pressure, whereas the monolayer must be heated to be removed. The fact that monolayer desorption is an activated process means that we can use TPD to probe the energetics. We used the following equation to calculate the activation energy of desorption from TPD experiments:

$$-\frac{d\theta}{dt}=\nu\theta^{n}\exp\left[-\frac{E_d}{RT}\right], \tag{7}$$

where R is the gas constant, ν is the pre-exponential factor, θ is the adsorbate coverage, n is the order of the desorption process, and E_d is the activation energy for desorption.[79,80]

A series of TPD spectra for propane dosed at 90 K on HOPG are shown in Fig. 7. A single peak appears around 115 K. The propane TPD spectra grow with a common leading edge and abrupt trailing edge, indicating zero order desorption.[81] Using zero order desorption kinetics, the activation energy for desorption of propane on HOPG is estimated to be 30 ± 2 kJ mol^{-1} (Fig. 10). The uncertainties arise in part from the accuracy of temperature measurements. The heat of vaporization of propane at its normal boiling point (230.9 K) is 19 kJ mol^{-1},[82] while integration of the heat capacity yields a value of 24 kJ mol^{-1} for the heat of vaporization at 100 K. This is smaller than the calculated activation energy and is consistent with the strong solid–fluid interaction for adsorbed propane. There is no evidence in the TPD spectra of bilayer or multilayer formation under present experimental conditions.

The isosteric heat of adsorption can be obtained experimentally from the following relationship:[83]

$$q_{st}=-R\left[\frac{\partial\ln P}{\partial(1/T)}\right]_{n}, \tag{8}$$

where q_{st} is the isosteric heat, T is the temperature, P is the pressure, and n is the coverage. Plots of $\ln P$ as a function of reciprocal absolute temperature at constant coverage are called adsorption isosteres and the isosteric heat of adsorption is determined by their slopes. Experiments performed at

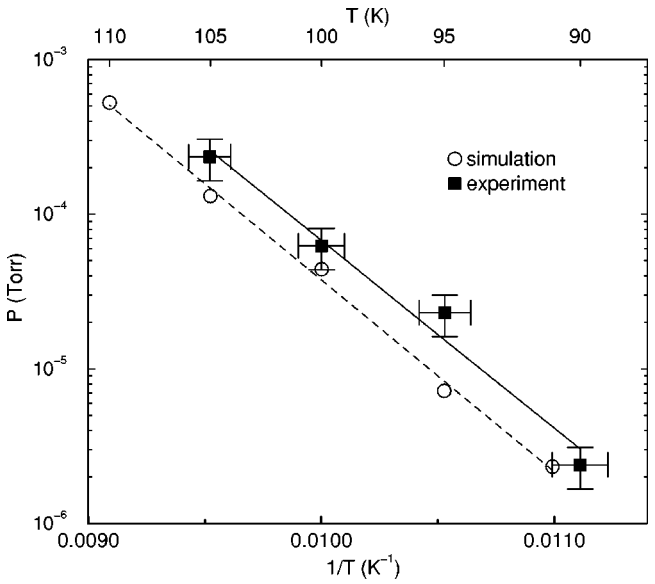

FIG. 11. Isosteres from experiments and GCMC simulations. The filled squares are from experiments and circles are from simulations. The dashed and solid lines are fits to the simulation and experimental data, respectively. The slopes of the lines give q_{st} through Eq. (8). The values are 23 ± 2 and 24 ± 1 kJ mol^{-1} from experiments and simulations, respectively.

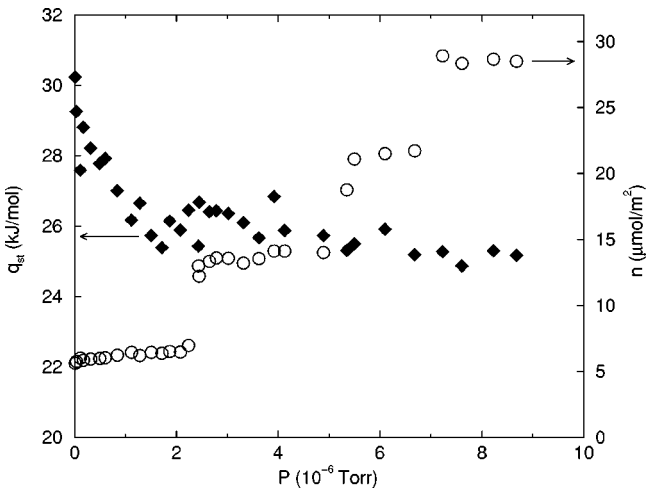

FIG. 12. Isosteric heat of adsorption (diamonds, left axis) and adsorption isotherm (circles, right axis) from simulations of propane on graphite at 91 K as a function of pressure. The values of q_{st} are computed from Eq. (5).

five temperatures (90, 95, 100, 105, and 110 K) allow determination of q_{st}. The average pressures where the second layer just begins to form at each temperature was used to construct a single isostere. For experiments at 110 K second layer formation was not observed at pressures up to 2×10^{-4} Torr, consistent with the simulations showing that the second layer forms at a pressure of about 5×10^{-4} Torr. The isosteres procedure can be applied to the isotherms calculated from simulations. The values of q_{st} from the isosteres [Eq. (8)] and the statistical method [Eq. (5)] should agree with each other, although it has been noted that measurements of q_{st} by different experimental methods are often in disagreement and differences of 10%–20% are common.[83]

The isosteres computed from experimental and simulation data are plotted in Fig. 11. The experimental values in Fig. 11 represent the average of several isotherm measurements and the error bars were estimated based on the scatter in the experimental data. The values of isosteric heat at bilayer formation determined from experimental and simulation data are in excellent agreement. The experimentally determined value of q_{st} is 23 ± 2 kJ mol^{-1}, while that calculated from simulation is 24 ± 1 kJ mol^{-1}.

The dependence of q_{st} on pressure at 91 K as computed from GCMC simulation through Eq. (5) is shown in Fig. 12. At lowest pressures simulated in our work, the isosteric heat of adsorption is estimated to be around 31 kJ mol^{-1}. This corresponds to complete monolayer coverage, although there is a slight increase in the coverage as the pressure increases before the transition pressure for the second layer. The value of $q_{st}\sim31$ kJ mol^{-1} implies a binding energy[3] of $q_{st}-RT/2\sim30.6$ kJ mol^{-1}, which is in excellent agreement with $E_d=30\pm2$ kJ mol^{-1} as measured from TPD. The increase in coverage in an apparently full monolayer will be addressed below. As the pressure increases q_{st} decreases to about 25 kJ mol^{-1}, with fairly large fluctuations, and is fairly independent of pressure through the formation of the bilayer and multilayers. For comparison, the isosteric heat at zero coverage is 27.9 kJ mol^{-1}, as computed from numerical integration.[28] The value of q_{st} computed from Eq. (5) around monolayer completion is in good agreement with the value computed from Eq. (8) from the experimental and simulation data. The isosteric heats of adsorption at 300 K were also calculated from simulations over a range of coverages. The value of the isosteric heat at zero coverage at 300 K is 25 kJ mol^{-1} from simulation and compares very well with the experimental data measured by Lal and Spencer in the range from 24.8 to 27.3 kJ mol^{-1}.[84] Agreement with the experimental data indicates that the energetics of the LS potential model are quite accurate, despite its simplicity.

In general, a pronounced decrease in q_{st} upon monolayer completion is expected because the adsorbate–adsorbate interactions in the first layer become more and more repulsive as the monolayer completes. When the first layer is completely filled subsequent molecules must occupy the second layer. Therefore, q_{st} is expected to drop because of the relatively weak interactions between the second layer molecules and the graphite surface. This type of behavior has been noted for fluids such as methane, hydrogen, nitrogen, and carbon dioxide on graphite.[24,85–89] We have plotted the isosteric heat and adsorption isotherm for methane on graphite at 77 K in Fig. 13 as an example. We have used the same parameters in these calculations for methane as those used by Jiang *et al.*,[24] but with a potential cutoff of 5 σ. Note that the isosteric heat drops dramatically upon completion of the monolayer and remains low until the second layer is substantially occupied. The coverage in the first layer remains essentially constant from a pressure of about 0.1 Torr until the second layer abruptly fills at a pressure of about 3 Torr. The isosteric heat from about 0.1 to 3 Torr is roughly constant with a value around 6.4 kJ mol^{-1}. This isosteric heat is due to molecules added to the second layer at zero coverage in the second layer, i.e., without any neighbors in the second

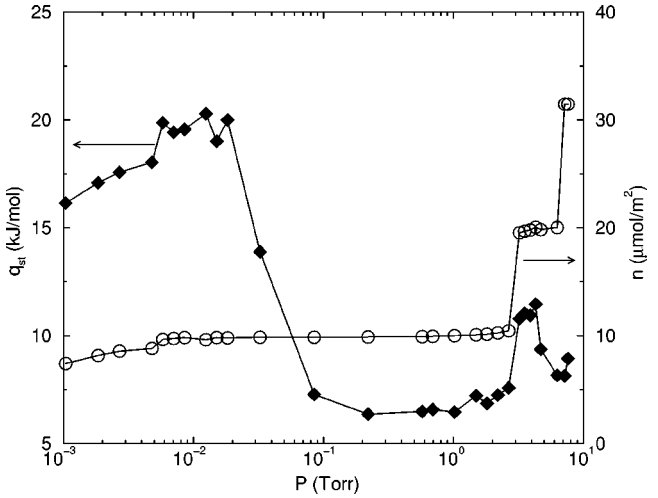

FIG. 13. Isosteric heat of adsorption (diamonds, left axis) and adsorption isotherm (circles, right axis) for methane on graphite at 77 K simulations. The lines are to guide the eye.

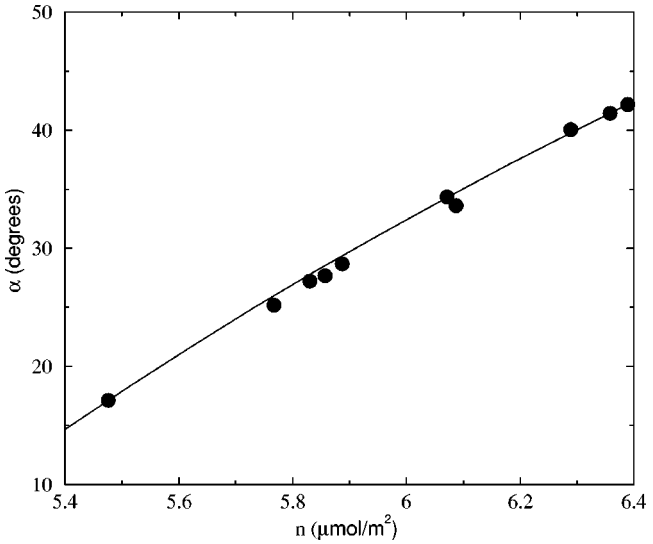

FIG. 14. The average angle between the plane of the propane molecule and the graphite basal plane as a function of coverage for the 91 K isotherm. The circles are the data from the simulations, the line is the calculation from Eq. (14).

layer. We have verified that the isosteric heat from 0.1 to about 3 Torr is due to addition of molecules into the second layer rather than in the first layer by computing the isosteric heat for a single methane molecule adsorbing on the frozen first layer of methane on graphite. This was done by numerical integration[28] with a resulting value of 6.1 kJ mol^{-1}, in good agreement with the plateau region of Fig. 13. It is generally accepted that the large drop in q_{st} on monolayer filling is due to the much lower solid–fluid interaction of molecules in the second layer. Note that q_{st} increases somewhat when the second layer becomes filled because of the attractive adsorbate–adsorbate interactions in the second layer. However, for propane on graphite q_{st} unexpectedly remains essentially constant as the bilayer and multilayers grow (Fig. 12).

C. Orientational ordering

In addition to the roughly constant isosteric heat as a function of coverage, another related phenomenon is the slight increase in coverage in the first layer with pressure after monolayer filling, but before second layer formation. This can be observed from simulations in Figs. 5, 6, and 8. The noise in the experiments makes it difficult to observe the increase in monolayer density experimentally. The increase in monolayer coverage with increasing pressure observed for propane is not observed for simple fluids such as methane (see Fig. 13).

Both the absence of a drop in the isosteric heat upon monolayer completion and the slight increase in coverage in the monolayer with pressure can be explained in terms of an observed orientational transition of the adsorbed propane molecules. The angles between the plane of the propane molecules and the graphite basal plane for each of the molecules in the first layer have been measured from the GCMC simulations. The average angle of the propane molecules adsorbed in the first layer at 91 K is shown in Fig. 14 as a function of coverage. We observe that the average angle of the propane molecules depends linearly on the pressure for coverages in the first layer. Note that this graph starts from a coverage that is close to the monolayer limit. At zero coverage propane will have an angle close to zero (parallel with the surface). Although only results for 91 K are shown in Fig. 14, the same linear increase in angle with coverage can be observed for all temperatures studied.

The rotation of propane in the first layer can be viewed as a monolayer roughening transition that facilitates the growth of the second layer. This is because the first molecules to adsorb in the second layer do not adsorb onto a ''bare'' surface, but one that has many CH_3 groups protruding into the second layer. These groups serve to increase the isosteric heat in the second layer over the value for adsorption onto a perfect $\alpha=0$ propane surface, where α is the average angle between the propane molecule and the graphite plane. We have verified this by comparing the energetics of a single propane molecule at 91 K on a relatively smooth propane monolayer and on a monolayer of propane molecules with an average angle of about 42°. The average angle for the monolayer molecules in the ''smooth'' surface was about 17°. We have computed the isosteric heat by performing Monte Carlo integrations of a single propane molecule interacting with the propane monolayer on graphite. This is analogous to the approach used by Cracknell and Nicholson[28] for computing the zero coverage isosteric heats. Our calculations yield the isosteric heat at zero coverage in the second layer on top of a full monolayer, given by

$$q_{st}^{0}=RT-N_a\frac{\int u_s(\mathbf{r},\boldsymbol{\omega})\exp[-\beta u_s(\mathbf{r},\boldsymbol{\omega})]d\mathbf{r}d\boldsymbol{\omega}}{\int \exp[-\beta u_s(\mathbf{r},\boldsymbol{\omega})]d\mathbf{r}d\boldsymbol{\omega}}, \qquad (9)$$

where u_s is the interaction potential between a propane molecule and the surface (graphite plus fixed monolayer), $\mathbf{r}$ is the center of mass, and $\boldsymbol{\omega}$ represents the orientation of the propane molecule, and the integrals are over the volume of the system and all orientations of the propane molecule. We have averaged the results from 11 separate Monte Carlo in-

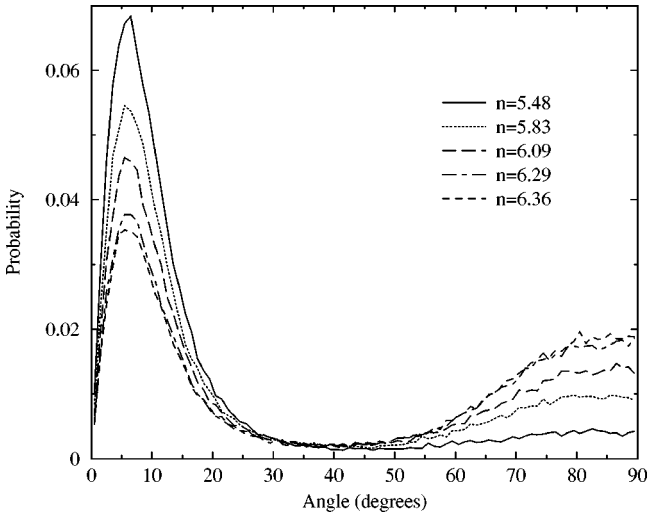

FIG. 15. The probability distribution for the angle between the plane of the propane molecule and the graphite basal plane for coverages in the monolayer regime.

tegrations for each surface. The results are $q_{st}=21.8\pm0.3$ kJ mol^{-1} for the "smooth" propane monolayer and $q_{st}=26.7\pm0.4$ kJ mol^{-1} for the "rough" surface. The uncertainty is the estimate for 1 standard deviation of the mean. The latter value is in excellent agreement with q_{st} computed from simulations at the second layer transition shown in Fig. 12. The increase in q_{st} in the second layer with increasing α produces an isosteric heat that is roughly independent of coverage from monolayer to bilayer, as observed in Fig. 12.

Orientational ordering of molecules in the monolayer has been previously noted for other systems. For example, Bottani *et al.* have observed that carbon dioxide exhibits a coverage dependence in the average tilt angle of CO_2 relative to the graphite basal plane,[89] and Raut *et al.* noted that *n*-butane begins to tilt at high coverages on Pt (111) at low temperature in order to accommodate a higher coverage in the monolayer.[90]

We have computed the probability of observing a given propane tilt angle as a function of coverage for the 91 K isotherm. The probability distribution is distinctly bimodal, with a peak at about $\alpha=8°$ and another broader peak centered at about $85°-90°$ (Fig. 15). The probability distribution indicates that molecules are very likely to be in one of two states, one relatively flat with $\alpha\sim0°$, and one almost perpendicular with $\alpha\sim90°$. There is a low probability that a molecule will have an angle between 30° and 50°. The relative population of the two peaks in the bimodal distribution is seen to shift from $\alpha\sim0°$ to $\alpha\sim90°$ as the coverage increases. However, this shift is apparently not an orientational phase transition. Snapshots reveal that the molecules that are oriented perpendicular to the surface are not clustered together, but appear fairly randomly over the surface of the monolayer.

The linear dependence of the average angles of the propane molecules on coverage can be explained by a simple geometric theory. At low monolayer coverages, the molecule has all three sites (two CH_3 and one CH_2) in contact with the graphite surface ($\alpha\sim0°$), whereas at higher monolayer coverages, only two sites contact the surface ($\alpha\sim90°$). As the propane monolayer fills, molecules rotate from 0° to 90°. Based on the potential model used in the simulation, we calculated that rotation of a single molecule in the monolayer from $\alpha=0°$ to 90° leads to an increase in the system internal energy of about $6-7$ kJ mol^{-1}. Insertion of a molecule from the gas phase into the monolayer decreases the internal energy of the system by about $30-40$ kJ mol^{-1}, depending on the configuration. Hence, it is energetically favorable to rotate several molecules in order to accommodate another propane molecule adsorbing on the surface. Geometrically, rotation of a small number of molecules from $\alpha=0°$ to 90° can provide enough surface area for the adsorption of a propane molecule from the gas phase onto the graphite surface. This accounts for the observation that the coverage in the first layer continues to increase slightly as the pressure increases. The increase in coverage with rotation can be quantified as follows. Assume that at some low pressure the total number of adsorbed propane molecules is N_l. Among these N_l molecules, N_0 molecules have an angle close to 0° (denoted α_0) and N_{90} molecules have an angle of about 90° (α_{90}) such that $N_l=N_0+N_{90}$. The average angle can be written as

$$\langle\alpha_l\rangle=\frac{N_0\alpha_0+(N_l-N_0)\alpha_{90}}{N_l}. \tag{10}$$

Solving for N_0 we have

$$N_0=\frac{\alpha_{90}-\langle\alpha_l\rangle}{\alpha_{90}-\alpha_0}N_l, \tag{11}$$

and likewise,

$$N_{90}=\frac{\langle\alpha_l\rangle-\alpha_0}{\alpha_{90}-\alpha_0}N_l. \tag{12}$$

At higher coverage, if the total number of adsorbed propane molecules is increased to N_h, we assume that N' of the N_0 molecules must rotate from α_0 to α_{90} in order to accommodate $\Delta N=N_h-N_l$ more molecules into the monolayer with an angle of $\alpha\sim90°$. The average angle in the higher coverage state is

$$\langle\alpha_h\rangle=\frac{(N_0-N')\alpha_0+(N_{90}+\Delta N+N')\alpha_{90}}{N_h}. \tag{13}$$

Insertion of an additional molecule into the monolayer with an angle of α_{90} requires that s molecules already in the monolayer be rotated from the α_0 to the α_{90} orientation, giving $N'=s\Delta N=s(N_h-N_l)$. Substituting N_0, N_{90}, N', and ΔN as functions of N_l and N_h into Eq. (13), we have

$$\langle\alpha_h\rangle=\frac{N_l}{N_h}\langle\alpha_l\rangle+\left(1-\frac{N_l}{N_h}\right)[(1+s)\alpha_{90}-s\alpha_0]. \tag{14}$$

The curve predicted by Eq. (14) for the average angle as a function of coverage is nonlinear. However, the function is approximately linear over a narrow range of coverage. In our simulations $N_l=5.48$ μmol/m^2 at the lowest pressure. The corresponding average angle is $\langle\alpha_l\rangle=17.1°$. At any coverage higher than N_l, denoted as N_h, the average angle is given by $\langle\alpha_h\rangle$ from Eq. (14). Equation (14) contains three

unknown parameters, α_0, α_{90}, and s. Nonlinear regression gives $\alpha_0 = 6°$, $\alpha_{90} = 85°$, and $s = 1.36$, when starting from reasonable initial guesses. The values of α_0 and α_{90} agree well with the data from Fig. 15. The fit to Eq. (14) gives a good match to the simulation data, as can be seen from Fig. 14, where the solid line is computed from Eq. (14) using the above values of the parameters.

V. CONCLUSION

We have presented experimental and computer simulation studies of propane adsorption on HOPG. The isosteric heat of adsorption was independently determined from experiments and simulation. The simulation results and experimental data are in good agreement for q_{st} near the 1–2 layering transition. The values of q_{st} computed from the isosteres method [Eq. (8)] and from the simulation statistical method [Eq. (5)] are in very good agreement. The 1–2 layering transition from 90 to 105 K appears to be first order. While the monolayer adsorption is irreversible on the time scale of the experiments, bilayer formation is quite reversible. Indeed, without an *in situ* probe (such as ODR) capable of operation at milliTorr pressure such phenomenon would not be observable, because the reduction of pressure to a range where most surface science techniques operate would lead to bilayer desorption. This underscores the versatility of ODR. The 1–2 layering transition pressures from experiments and simulations are generally in good agreement, considering the uncertainty in the experimental pressure and temperature measurements and the approximate nature of the potential models used in the simulations. The value of the 1–2 layering transition pressure from simulations was found to be very sensitive to the fluid–fluid interaction potential. The sharpness of the transition (first order or continuous) was not affected by the choice of a fluid–fluid potential, whereas a 5% decrease in the solid–fluid potential is apparently sufficient to change the transition from first order to continuous at 100 K. However, changes in the solid–fluid potential have comparatively moderate effect on the pressure at which the transition takes place. These observations underscore the importance of the accuracy of the fluid–fluid potential if one is interested in locating accurately the transition pressure.

We have observed unexpected behavior for the isosteric heat of adsorption across the first and second layer transitions. For simple fluids the isosteric heat exhibits a dramatic drop upon completion of the first layer and a slight recovery in q_{st} at the formation of the second layer. In contrast, the isosteric heat for propane is almost constant from monolayer completion to formation of the multilayer. An unusual slight increase in the monolayer coverage (before the onset of the second layer transition) was observed. Both of these phenomena can be explained by the orientational transition observed in simulations. Individual propane molecules rotate from orientations that are parallel to the graphite surface to an orientation almost perpendicular to the surface, having one methyl group pointing up from the monolayer. This orientational change provides a more attractive (roughened) surface for second layer adsorption, thereby increasing q_{st} and the coverage in the monolayer. The simulation data show that the average angle of propane in the monolayer depends linearly on coverage, which can be explained in terms of a simple geometric model.

ACKNOWLEDGMENTS

The authors gratefully acknowledge helpful discussions with Milton Cole and Haskell Taub. This work was supported by the National Energy Technology Laboratory, the U.S. DOE (Grant No. DE-FG26-98FT40119) and the NSF (Grant No. CTS-9702239). Calculations were performed at the Center for Molecular and Materials Simulation at the University of Pittsburgh.

[1] M. Ammann, M. Kalbare, D. T. Jost, L. Tobler, E. Rossler, D. Piguet, H. W. Gaggeler, and U. Baltensperger, Nature (London) **395**, 157 (1998).
[2] J. A. Korpiel and R. Vidic, Environ. Sci. Technol. **31**, 2319 (1997).
[3] D. M. Ruthven, *Principles of Adsorption and Adsorption Processes* (Wiley, New York, 1984).
[4] A. J. Gellman, Curr. Opin. Colloid Interface Sci. **3**, 368 (1998).
[5] D. P. Valenzuela and A. L. Myers, *Adsorption Equilibrium Data Handbook* (Prentice–Hall, Englewood Cliffs, N.J., 1989).
[6] H. S. Youn, X. F. Meng, and G. B. Hess, Phys. Rev. B **48**, 14556 (1993).
[7] W. A. Steele, Chem. Rev. **93**, 2355 (1993).
[8] G. Vidali, G. Ihm, H.-Y. Kim, and M. W. Cole, Surf. Sci. Rep. **12**, 133 (1991).
[9] G. Zimmerli and M. H. W. Chan, Phys. Rev. B **45**, 9347 (1992).
[10] G. B. Hess, in *Phase Transitions in Surface Films 2*, edited by H. Taub, G. Torzo, H. J. Lauter, and S. C. Fain, Jr. (Plenum, New York, 1991).
[11] P. A. Rowntree, G. Scoles, and J. C. Ruiz-Suáres, J. Phys. Chem. **94**, 8511 (1990).
[12] J. C. Ruiz-Suáres, M. L. Klein, M. A. Moller, P. A. Rowntree, G. Scoles, and J. Xu, Phys. Rev. Lett. **61**, 710 (1988).
[13] S. Kwon, R. D. Vidic, X. Zhao, J. K. Johnson, and E. Borguet, Langmuir **18**, 2595 (2002).
[14] M. Dorko, T. Bryden, and S. Garrett, J. Phys. Chem. B **104**, 11695 (2000).
[15] K. R. Paserba and A. J. Gellman, J. Chem. Phys. **115**, 6737 (2001).
[16] K. R. Paserba and A. J. Gellman, Phys. Rev. Lett. **86**, 4338 (2001).
[17] D. M. Cyr, B. Venkataraman, and G. W. Flynn, Chem. Mater. **8**, 1600 (1996).
[18] M. J. Lysek, M. A. L. Madrid, P. K. Day, and D. L. Goodstein, Phys. Rev. B **47**, 7389 (1993).
[19] H. S. Nham and G. B. Hess, Phys. Rev. B **38**, 5166 (1988).
[20] Q. M. Zhang, Y. P. Feng, H. K. Kim, and M. H. W. Chan, Phys. Rev. Lett. **57**, 1456 (1986).
[21] M. Drir, H. S. Nham, and G. B. Hess, Phys. Rev. B **33**, 5145 (1986).
[22] M. A. Lee, M. T. Alkafaji, and A. D. Migone, Langmuir **13**, 2791 (1997).
[23] B. E. Matthies, Ph.D. thesis, University of Missouri-Columbia, Missouri 1999.
[24] S. Jiang, K. E. Gubbins, and J. A. Zollweg, Mol. Phys. **83**, 103 (1993).
[25] A. V. Klochko, E. N. Brodskaya, and E. M. Piotrovskaya, Langmuir **15**, 545 (1999).
[26] R. F. Cracknell and D. Nicholson, Mol. Phys. **80**, 885 (1993).
[27] R. F. Cracknell and D. Nicholson, Mol. Simul. **13**, 161 (1994).
[28] R. F. Cracknell and D. Nicholson, J. Chem. Soc., Faraday Trans. **90**, 1487 (1994).
[29] R. F. Cracknell and D. Nicholson, Adsorption **1**, 7 (1995).
[30] L. D. Gelb and K. E. Gubbins, Stud. Surf. Sci. Catal. **128**, 61 (2000).
[31] M. Sliwinska-Bartkowiak, J. Gras, R. Sikorski, G. Dudziak, R. Radhakrishnan, and K. E. Gubbins, Stud. Surf. Sci. Catal. **128**, 141 (2000).
[32] K. T. Thomson and K. E. Gubbins, Langmuir **16**, 5761 (2000).
[33] M. J. Bojan and R. van Sloonten, Sep. Sci. Technol. **27**, 1837 (1992).
[34] J. L. Soto and A. L. Myers, Mol. Phys. **42**, 971 (1981).
[35] G. B. Woods, A. Z. Panagiotopoulos, and J. S. Rowlinson, Mol. Phys. **63**, 49 (1988).
[36] S. Yashonath, J. M. Thomas, A. K. Nowak, and A. K. Cheetham, Nature (London) **331**, 601 (1988).
[37] S. Yashonath, P. Demontis, and M. L. Klein, Chem. Phys. Lett. **153**, 551 (1988).

[38] G. B. Woods and J. S. Rowlinson, J. Chem. Soc., Faraday Trans. 2 **85**, 765 (1989).
[39] R. L. June, A. T. Bell, and D. N. Theodorou, J. Phys. Chem. **94**, 1508 (1990).
[40] F. Karavias and A. L. Myers, Mol. Simul. **8**, 23 (1991).
[41] F. Karavias and A. L. Myers, Mol. Simul. **8**, 51 (1991).
[42] R. Q. Snurr, A. T. Bell, and D. N. Theororou, J. Phys. Chem. **97**, 13742 (1993).
[43] M. D. LeVan, *Fundamentals of Adsorption: Proceedings of the Fifth International Conference on Fundamentals of Adsorption* (Kluwer Academic, Boston, MA, 1996).
[44] R. J. M. Pellenq, B. Tavitian, D. Espinat, and A. H. Fuchs, Langmuir **12**, 4768 (1996).
[45] M. Heuchel, R. Q. Snurr, and E. Buss, Langmuir **13**, 6795 (1997).
[46] L. F. Gladden, M. Hargreaves, and P. Alexander, Chem. Eng. J. **74**, 57 (1999).
[47] M. D. Macedonia and E. J. Maginn, Fluid Phase Equilib. **160**, 19 (1999).
[48] F. Marinelli, Y. Grillet, and R. J. M. Pellenq, Mol. Phys. **97**, 1207 (1999).
[49] T. J. Hou, L. L. Zhu, and X. J. Xu, J. Phys. Chem. B **104**, 9356 (2000).
[50] R. J. M. Pellenq, S. Rodts, V. Pasquier, A. Delville, and P. Levitz, Adsorption **6**, 241 (2000).
[51] E. M. Aydt and R. Hentschke, Ber. Bunsenges. Phys. Chem. **101**, 79 (1997).
[52] G. W. Wu and K. Y. Chan, Fluid Phase Equilib. **132**, 21 (1997).
[53] M. Pierce and E. Manousakis, Phys. Rev. B **63**, 144524 (2001).
[54] M. Pierce and E. Manousakis, Phys. Rev. B **59**, 3802 (1999).
[55] M. Pierce and E. Manousakis, Phys. Rev. Lett. **81**, 156 (1998).
[56] Q. Y. Wang and J. K. Johnson, Mol. Phys. **95**, 299 (1998).
[57] Q. Y. Wang and J. K. Johnson, Int. J. Thermophys. **19**, 835 (1998).
[58] J. J. Potoff and J. I. Siepmann, Phys. Rev. Lett. **85**, 3460 (2000).
[59] F. Y. Hansen and H. Taub, Inorg. Mater. (Transl. of Neorg. Mater.) **35**, 586 (1999).
[60] S. Balasubramanian, M. L. Klein, and J. I. Siepmann, J. Chem. Phys. **103**, 3184 (1995).
[61] R. Hentschke and R. G. Winkler, J. Chem. Phys. **99**, 5528 (1993).
[62] R. Hentschke, B. L. Schurmann, and J. P. Rabe, J. Chem. Phys. **96**, 6213 (1992).
[63] R. Loring and G. H. Findenegg, J. Colloid Interface Sci. **84**, 355 (1981).
[64] G. H. Findenegg and R. Loring, J. Chem. Phys. **81**, 3270 (1984).
[65] P. Glanz, B. Korne, and G. H. Findenegg, Adsorpt. Sci. Technol. **1**, 183 (1984).
[66] B. A. Younglove and J. F. Ely, J. Phys. Chem. Ref. Data **16**, 577 (1987).
[67] S. Kwon, R. D. Vidic, and E. Borguet, Carbon **40**, 2351 (2002).
[68] R. Lustig and W. A. Steele, Mol. Phys. **65**, 475 (1988).
[69] W. L. Jorgensen, J. D. Madura, and C. J. Swenson, J. Am. Chem. Soc. **106**, 813 (1984).
[70] M. G. Martin and J. I. Siepmann, J. Phys. Chem. B **102**, 2569 (1998).
[71] S. K. Nath, F. A. Escobedo, and J. J. de Pablo, J. Chem. Phys. **108**, 9905 (1998).
[72] J. I. Siepmann, S. Karaborni, and B. Smit, Nature (London) **365**, 330 (1993).
[73] M. P. Allen and D. J. Tildesley, *Computer Simulation of Liquids* (Clarendon, Oxford, 1987).
[74] J. I. Siepmann (personal communication).
[75] N. B. Vargaftik, Y. K. Vinogradov, and V. S. Yargin, *Handbook of Physical Properties of Liquids and Gases: Pure Substances and Mixtures* (Begell House, New York, 1996).
[76] W. A. Steele, Surf. Sci. **36**, 317 (1973).
[77] D. Nicholson and N. G. Parsonage, *Computer Simulation and the Statistical Mechanics of Adsorption* (Academic, London, 1982).
[78] D. P. Woodruff and T. A. Delchar, *Modern Techniques of Surface Science* (Cambridge University Press, Cambridge, 1986).
[79] K. Witman, D. Borgmann, and G. Wedler, Appl. Phys. A: Solids Surf. **51**, 132 (1990).
[80] P. A. Redhead, Vacuum **12**, 203 (1962).
[81] A. M. de Jong and J. Niemantsverdriet, Surf. Sci. **233**, 355 (1990).
[82] D. R. Lide, *CRC Handbook of Chemistry and Physics*, 78th ed. (CRC, Cleveland, OH, 1997).
[83] D. M. Shen, F. S. M. Bülow, M. Engelhard, and A. L. Myers, Adsorption **6**, 275 (2000).
[84] M. Lal and D. Spencer, J. Chem. Soc., Faraday Trans. 2 **70**, 910 (1973).
[85] Q. Wang and J. K. Johnson, Mol. Phys. **95**, 299 (1998).
[86] J. G. Daunt, S. G. Hedge, S. P. Tsui, and E. Lerner, J. Low Temp. Phys. **44**, 207 (1981).
[87] E. L. Pace and A. R. Siebert, J. Phys. Chem. **63**, 1398 (1959).
[88] E. J. Bottani and V. A. Bakaev, Langmuir **10**, 1550 (1994).
[89] E. J. Bottani, V. Bakaev, and W. Steele, Chem. Eng. Sci. **49**, 2931 (1994).
[90] J. S. Raut, D. S. Sholl, and K. A. Fichthorn, Surf. Sci. **389**, 88 (1997).